Supporting Information

Obtaining Giant Rashba-Dresselhaus Spin Splitting in Two-Dimensional Chiral Metal-Organic Frameworks

Shanshan Liu,[a] Ke Xu,[*c] Xingxing Li,[*ab] Qunxiang Li [ab] and Jinlong Yang [ab]

[a]Key Laboratory of Precision and Intelligent Chemistry, University of Science and Technology of China, Hefei, Anhui 230026, China

[b]Hefei National Research Center for Physical Sciences at the Microscale, University of Science and Technology of China, Hefei, Anhui 230026, China

[c]Hubei Key Laboratory of Low Dimensional Optoelectronic Materials and Devices, School of Physics and Electronic Engineering, Hubei University of Arts and Science, Xiangyang, 441053, China

*E-mail: xuke@hbuas.edu.cn

*E-mail: lixx@ustc.edu.cn

Note S1. Group theory analysis

Reduction of reducible representation:

To compute the characters for the full rotation group, we use the formula [1]:

$$\chi^j(\alpha) = \frac{\sin((j + 1/2)\theta)}{\sin(\theta/2)} \quad (S1)$$

where χ is the character of the reducible representation Γ, θ is the rotation angle.

For $j = 1/2$, 3/2 and 5/2 states, we have:

$$\chi^{1/2}(\theta) = \frac{\sin(\theta)}{\sin(\theta/2)}$$

$$\chi^{3/2}(\theta) = \frac{\sin(2\theta)}{\sin(\theta/2)} \quad (S2)$$

$$\chi^{5/2}(\theta) = \frac{\sin(3\theta)}{\sin(\theta/2)}$$

C_2 double group (Table S5):

For the $E, \bar{E}, C_2, \bar{E}C_2$ symmetry operations of the C_2 double group, the corresponding rotation angle θ is 0, 2π, π, $-\pi$. Substitute into Eq. S2 to get:

C_2^D	E	$\bar{E}$	C_2	$\bar{E}C_2$
$\Gamma^{1/2}$	2	-2	0	0
$\Gamma^{3/2}$	4	-4	0	0
$\Gamma^{5/2}$	6	-6	0	0

Reducible representations can be transformed into direct sums of irreducible representations. The following formula can calculate the number of occurrences of the i-th irreducible representation:

$$a_i = \frac{1}{h}\sum_{\hat{R}}^{h} \chi_i(\hat{R})^* \chi_\Gamma(\hat{R}) \quad (S3)$$

where h is the order of the group, $\hat{R}$ is the symmetry operation, χ_i is the character of the matrix corresponding to irreducible representation Γ_i, and χ_Γ is the character of the matrix corresponding to reducible representation Γ.

From Eq. S3, Reducible representations Γ is reduced to:

$$\Gamma^{1/2} = \Gamma_3 \oplus \Gamma_4$$

$$\Gamma^{3/2} = 2\Gamma_3 \oplus 2\Gamma_4 \quad (S4)$$

$$\Gamma^{5/2} = 3\Gamma_3 \oplus 3\Gamma_4$$

D_4 double group (Table S6):

For the $E, \bar{E}, C_4, \bar{E}C_4, C_2, \bar{E}C_2$ symmetry operations of the D_4 double group, the corresponding rotation angle θ is 0, 2π, $\pi/4$, $-\pi/4$, π, $-\pi$. Substitute into Eq. S2 to get:

D_4^D	E	$\bar{E}$	$2C_4$	$2\bar{E}C_4$	$C_2, \bar{E}C_2$	$2C_2', 2\bar{E}C_2'$	$2C_2'', 2\bar{E}C_2''$
$\Gamma^{1/2}$	2	-2	$\sqrt{2}$	$-\sqrt{2}$	0	0	0
$\Gamma^{3/2}$	4	-4	0	0	0	0	0
$\Gamma^{5/2}$	6	-6	$-\sqrt{2}$	$\sqrt{2}$	0	0	0

Similarly, according to Eq. S3, we can reduce the reducible representation to:

$$\Gamma^{1/2} = \Gamma_6$$

$$\Gamma^{3/2} = \Gamma_6 \oplus \Gamma_7 \tag{S5}$$

$$\Gamma^{5/2} = \Gamma_6 \oplus 2\Gamma_7$$

In the case of free atoms, if electron spin is not considered, the effective Hamiltonian symmetry group for the system is the full rotation group $O(3)$, and the l-state degeneracy is given by $2(2l + 1)$. When the spin-orbit coupling is further considered, the effective Hamiltonian symmetry group is the $SU(2)$ group, and the atomic state of the l-state will be divided into two energy levels ($j = l \pm 1/2$), each with a degeneracy degree of $2j+1$. When this free atom is placed in a surrounding crystal environment with point group symmetry, the Hamiltonian symmetry is reduced to that of the point group symmetry in the environment due to the interaction between the electron and its surroundings. At this time, the original degenerate energy level with a degeneracy of $2j+1$ will be further split, and the electronic state will be labeled with an irreducible representation of the point group.

In Fig. 4b, we only consider the p-state for the conduction band, which corresponds to $l = 1$. This state is split into two energy levels, $j = 1/2$ and $3/2$. When the atomic state is placed in a surrounding crystal environment with C_2 double point group symmetry, $\Gamma^{1/2}$ and $\Gamma^{3/2}$ can be reduced to $\Gamma_3 \oplus \Gamma_4$ and $2\Gamma_3 \oplus 2\Gamma_4$ (Eq. S4) respectively. It is worth mentioning that for the $j = 3/2$ state (with quadruple degeneracy), it will be decomposed into two $\Gamma_3 \oplus \Gamma_4$, which is not fully plotted in Fig. 4b. Regarding the valence band, we only consider the d-state ($l = 2$), which is split into two energy levels, $j = 3/2$ and $5/2$, and the corresponding $\Gamma^{3/2}$ and $\Gamma^{5/2}$ can be reduced to $2\Gamma_3 \oplus 2\Gamma_4$ and $3\Gamma_3 \oplus 3\Gamma_4$ (Eq. S4). Likewise, the $j = 5/2$ state (with six-fold degeneracy) and the $j = 3/2$ state (with quadruple degeneracy), are not fully plotted in Fig. 4b.

In Fig. 4d, we focus on the p-state ($l = 1$) at the conduction band. This state is split into two energy levels $j = 1/2$ and $3/2$. In a crystal environment with D_4 double point group symmetry, $\Gamma^{1/2}$ and $\Gamma^{3/2}$ can be reduced to Γ_6 and $\Gamma_6 \oplus \Gamma_7$ (Eq. S5) respectively. Regarding the valence band, we only consider the d-state ($l = 2$). This state is divided into two energy levels $j = 3/2$ and $5/2$, and the corresponding $\Gamma^{3/2}$ and $\Gamma^{5/2}$ can be reduced to $\Gamma_6 \oplus \Gamma_7$ and $\Gamma_6 \oplus 2\Gamma_7$ (Eq. S5) respectively.

Basis functions of the double-valued representations:

When the SOC effect is included, the spin-up and down states will be entangled together to form a two-component spinor. Therefore, it is necessary to use the projection operator under the double-valued representations to obtain the basis of the irreducible representations.

To compute the basis functions of the double-valued representations, the projection operator for irreducible representations (IR) can be used:

$$P^{\Gamma_i} = \frac{l_{\Gamma_i}}{h} \sum_R \chi_{\Gamma_i}(R)^* P_R P_S \#(S6)$$

where l_{Γ_i} is the dimension of the irreducible representation Γ_i, h is the order of the group, χ_{Γ_i} is the character of the irreducible representation, R is the symmetry operation, P_R and P_s correspond to the representation matrices of orbit and spin respectively.[2]

Take the D_4 double group as an example: (Table S6)

First, find the spin $\frac{1}{2}$ p-orbital basis of Γ_6 IR:

$$P^{\Gamma_6} \begin{bmatrix} p_x \\ p_y \\ p_z \end{bmatrix} \otimes \begin{bmatrix} \uparrow \\ \downarrow \end{bmatrix} = \frac{1}{4} \begin{bmatrix} p_x\uparrow \\ p_x\downarrow \\ p_y\uparrow \\ p_y\downarrow \\ p_z\uparrow \\ p_z\downarrow \end{bmatrix} + \frac{1}{4} \begin{bmatrix} ip_y\uparrow \\ -ip_y\downarrow \\ -ip_x\uparrow \\ ip_x\downarrow \\ p_z\uparrow \\ p_z\downarrow \end{bmatrix} \#(S7)$$

From Eq. S7, we find two doubly-degenerate basis of Γ_6 IR are: $\left\{\frac{1}{\sqrt{2}}(p_x+ip_y)\uparrow,\frac{1}{\sqrt{2}}(p_x-ip_y)\downarrow\right\}$, $\{p_z\uparrow,p_z\downarrow\}$

Second, find the spin $\frac{1}{2}$ p-orbital basis of Γ_7 IR:

$$\hat{P}^{\Gamma_7}\begin{bmatrix}p_x\\p_y\\p_z\end{bmatrix}\otimes\begin{bmatrix}\uparrow\\\downarrow\end{bmatrix}=\frac{1}{4}\begin{bmatrix}p_x\uparrow\\p_x\downarrow\\p_y\uparrow\\p_y\downarrow\\p_z\uparrow\\p_z\downarrow\end{bmatrix}+\frac{1}{4}\begin{bmatrix}-ip_y\uparrow\\ip_y\downarrow\\ip_x\uparrow\\-ip_x\downarrow\\-p_z\uparrow\\-p_z\downarrow\end{bmatrix}\#(S8)$$

From Eq. S8, we find one doubly-degenerate basis of Γ_7 IR are: $\left\{\frac{1}{\sqrt{2}}(p_x+ip_y)\uparrow,\frac{1}{\sqrt{2}}(p_x-ip_y)\downarrow\right\}$

Third, find the spin $\frac{1}{2}$ d-orbital basis of Γ_6 IR:

$$\hat{P}^{\Gamma_6}\begin{bmatrix}d_{z^2}\\d_{xz}\\d_{yz}\\d_{x^2-y^2}\\d_{xy}\end{bmatrix}\otimes\begin{bmatrix}\uparrow\\\downarrow\end{bmatrix}=\frac{1}{2}\begin{bmatrix}d_{z^2}\uparrow\\d_{z^2}\downarrow\\(d_{xz}+id_{yz})\uparrow\\(d_{xz}-id_{yz})\downarrow\\(d_{yz}-id_{xz})\uparrow\\(d_{yz}+id_{xz})\downarrow\\0\\0\\0\\0\end{bmatrix}\#(S9)$$

From Eq. S9, we find two doubly-degenerate basis of Γ_6 IR are: $\left\{d_{z^2}\uparrow,d_{z^2}\downarrow\right\}$, $\left\{\frac{1}{\sqrt{2}}(d_{xz}+id_{yz})\uparrow,\frac{1}{\sqrt{2}}(d_{xz}-id_{yz})\downarrow\right\}$

Last, find the spin $\frac{1}{2}$ d-orbital basis of Γ_7 IR:

$$\hat{P}^{\Gamma_7}\begin{bmatrix}d_{z^2}\\d_{xz}\\d_{yz}\\d_{x^2-y^2}\\d_{xy}\end{bmatrix}\otimes\begin{bmatrix}\uparrow\\\downarrow\end{bmatrix}=\frac{1}{4}\begin{bmatrix}0\\0\\(d_{xz}-id_{yz})\uparrow\\(d_{xz}+id_{yz})\downarrow\\(d_{yz}+id_{xz})\uparrow\\(d_{yz}-id_{xz})\downarrow\\d_{x^2-y^2}\uparrow\\d_{x^2-y^2}\downarrow\\2d_{xy}\uparrow\\2d_{xy}\downarrow\end{bmatrix}\#(S10)$$

From Eq. S10, we find three doubly-degenerate basis of Γ_7 IR are: $\left\{\frac{1}{\sqrt{2}}(d_{xz}+id_{yz})\uparrow,\frac{1}{\sqrt{2}}(d_{xz}-id_{yz})\downarrow\right\}$, $\left\{d_{x^2-y^2}\uparrow,d_{x^2-y^2}\downarrow\right\}$, $\{d_{xy}\uparrow,d_{xy}\downarrow\}$

Note S2. A possible route for the experimental synthesis

Here, we provide a possible route for the experimental synthesis of 2D chiral MOFs OsH$_2$(bipyridine_X_Y), where bipyridine_X_Y represents a series of axially chiral ligands 4,4'-bipyridines.[3]

MOF nanosheets can be synthesized via the bottom-up method.[4] The bottom-up method aims to synthesize MOF nanosheets using metals and organic precursors directly. In this process, the vertical directional growth is restricted while the lateral direction is not affected. The corresponding methods include interfacial synthesis,[5] three-layer synthesis,[6] surfactant-assisted synthesis,[7] modulated synthesis,[8] and sonication synthesis, etc.[9]

For our OsH$_2$(bipyridine_X_Y) nanosheets, first, the laser-ablated Os atoms and H$_2$ react in pure H$_2$ and solid neon/argon matrixes. Osmium atom reactions with hydrogen in excess neon/argon produce OsH$_2$ molecule.[10]

Next, the bipyridine_X_Y molecules and the OsH$_2$ are transferred onto an appropriate substrate (e.g., Si wafer)[11] by molecular layer deposition (MLD).[12] The bipyridine_X_Y molecules will form coordination complexes with the OsH$_2$ molecule. By adjusting the temperature, the metal-ligand ratio can be precisely controlled.[13]

Finally, after an annealing process under strict humidity control conditions, self-assembly takes place on the surface of the substrate to form the target MOF OsH$_2$(bipyridine_X_Y) with a specific structure.[14,15]
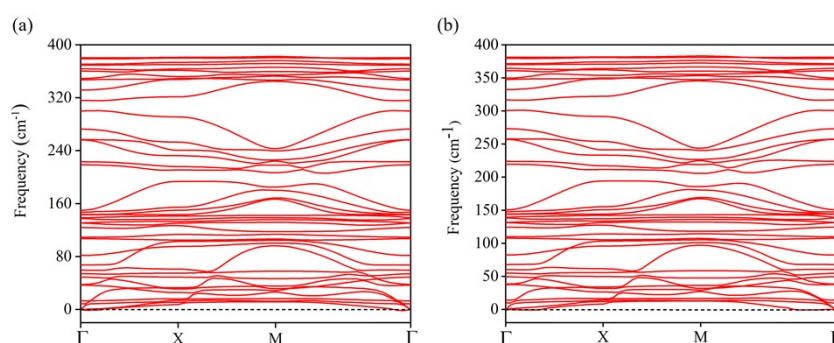

Fig. S1. Phonon spectra of OsH$_2$(bipyridine_CN) computed with (a) 2×2×1, and (b) 3×3×1 supercells, respectively. The calculation shows that the maximum imaginary frequency is reduced from 1.16 cm^{-1} with a 2×2×1 supercell to 0.78 cm^{-1} with a 3×3×1 supercell. These unphysically small imaginary frequencies are caused by size and boundary effects, and a similar phenomenon has also been observed in other reported MOFs [*J. Am. Chem. Soc.*, 2023, **145**, 7869−7878; *Nano Lett.*, 2022, **22**, 1573−1579; *J. Am. Chem. Soc.*, 2023, **145**, 2485−2491]. These small imaginary frequencies can theoretically be eliminated in larger supercells. Nevertheless, using supercells larger than 3×3×1 significantly increases the computing resources; hence, we only calculate phonon spectra with 3×3×1 supercells.
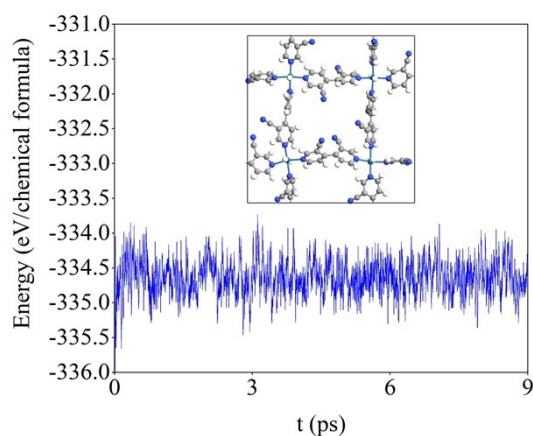
Fig. S2. The total potential energy fluctuations of $OsH_2(bipyridine\_CN)$ during ab initio molecular dynamics simulations using a 2×2×1 supercell at 600K.
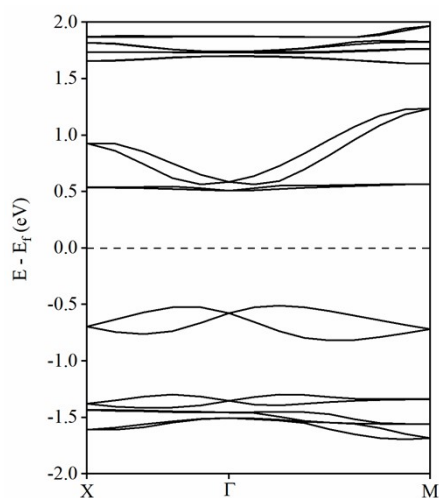
Fig. S3. HSE06+SOC band structure of 2D $OsH_2(bipyridine\_CN)$.

Fig. S4. (a) Possible path and energy barrier for the transition from structure **RR** to **RS** and **RS** to **SS**. (b) Different chirality of ligands in the structure of $OsH_2(bipyridine\_CN)$. Band structures calculated with (c) PBE+SOC of $OsH_2(bipyridine\_CN)$. The spin texture of (d) upper and lower Rashba bands in the VB of $OsH_2(bipyridine\_CN)$.

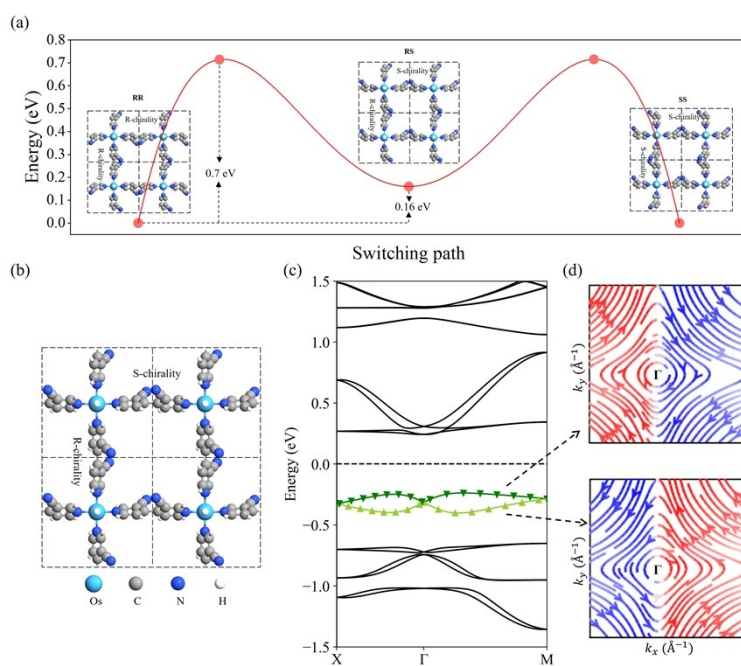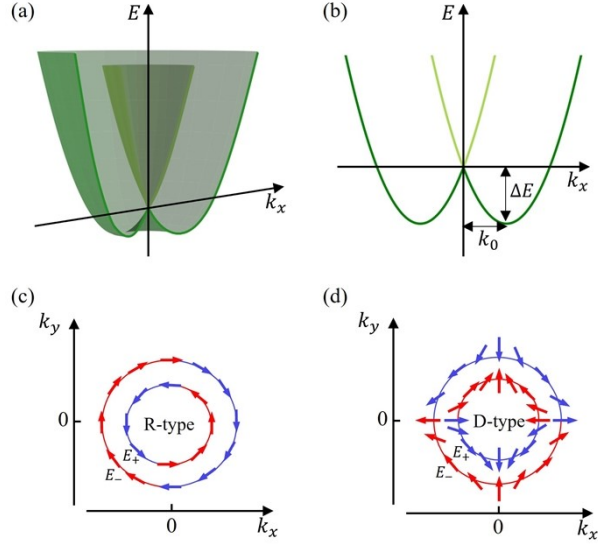Fig. S5. R-D band splitting and spin texture schematic diagram: (a) three-dimensional view. (b) two-dimensional view, ΔE is the energy difference between the energies of the peak and the degenerate energy at the high symmetry point, and k_0 is the momentum offset between the peak and the high symmetry point. (c) spin texture characteristic of the Rashba splitting (R-type) and (d) the Dresselhaus splitting (D-type) in the k_x-k_y plane, in which E_+ (E_-) denotes the upper (lower) branch, meanwhile the red (blue) color represents the positive (negative) spin component s_y.

Table S1. Parameters of CMOFs materials being calculated in Step I: material type, space group, band gap $E_g^{PBE + SOC}$, and ΔE in the valence band or conduction band (CB) at the Γ point.

Material	Non-magnetic semiconductor	Space group	$E_g^{PBE + SOC}$ (eV)	ΔE (meV)
SrCl$_2$(bipyridine_I)	Yes	$C2$	2.19	0.35
YCl$_2$(bipyridine_I)	Magnetic	-	-	-
ZrCl$_2$(bipyridine_I)	Magnetic	-	-	-
NbCl$_2$(bipyridine_I)	Magnetic	-	-	-
MoCl$_2$(bipyridine_I)	Magnetic	-	-	-
TcCl$_2$(bipyridine_I)	Magnetic	-	-	-
RuCl$_2$(bipyridine_I)	Yes	$C2$	1.45	0.50
RhCl$_2$(bipyridine_I)	Magnetic	-	-	-
PdCl$_2$(bipyridine_I)	Yes	$C2$	0.74	0.02(CB)
AgCl$_2$(bipyridine_I)	Magnetic	-	-	-
CdCl$_2$(bipyridine_I)	Yes	$C2$	2.53	0.15
SnCl$_2$(bipyridine_I)	Yes	$C2$	0.99	0.01
BaCl$_2$(bipyridine_I)	Yes	$C2$	1.85	0.02
HfCl$_2$(bipyridine_I)	Metal	-	-	-
TaCl$_2$(bipyridine_I)	Magnetic	-	-	-
WCl$_2$(bipyridine_I)	Magnetic	-	-	-
ReCl$_2$(bipyridine_I)	Magnetic	-	-	-
OsCl$_2$(bipyridine_I)	Yes	$C2$	1.2	3.20
IrCl$_2$(bipyridine_I)	Magnetic	-	-	-
PtCl$_2$(bipyridine_I)	Yes	$C2$	0.42	0.35(CB)

$AuCl_2$(bipyridine_I)	Magnetic	-	-	-
$HgCl_2$(bipyridine_I)	Yes	$C2$	2.45	0.05
$PbCl_2$(bipyridine_I)	Yes	$C2$	1.54	0.10

Table S2. Parameters of CMOFs materials being calculated in Step II: space group, band gap $E_g^{PBE+SOC}$, the symmetry at Γ in the VB and CB, ΔE, and the R-D coupling constant α in the valence band at the Γ point.

Material	Space group	$E_g^{PBE+SOC}$ (eV)	Same symmetry	ΔE (meV)	α (eVÅ)
OsI_2(bipyridine_I)	$C2$	1.46	No	2.6	0.05
$OsBr_2$(bipyridine_I)	$C2$	1.34	No	0.8	0.05
$OsCl_2$(bipyridine_I)	$C2$	1.20	No	3.2	0.12
OsF_2(bipyridine_I)	$C2$	0.64	Yes	11.5	0.38
$Os(CN)_2$(bipyridine_I)	$C2$	1.30	Yes	34.9	0.48
OsH_2(bipyridine_I)	$C2$	0.88	Yes	43.5	0.73

Table S3. Parameters of CMOFs materials being calculated in Step III: space group, band gap $E_g^{PBE+SOC}$, the symmetry at Γ in the VB and CB, ΔE, and the R-D coupling constant α in the valence band at the Γ point.

Material	Space group	$E_g^{PBE+SOC}$ (eV)	Same symmetry	ΔE (meV)	α (eVÅ)
OsH_2(bipyridine_CH$_3$_I)	$P1$	1.20	Yes	3.9	0.17
OsH_2(bipyridine_CH$_3$_NH$_2$)	$P1$	1.10	Yes	16.6	0.42
OsH_2(bipyridine_NH$_2$)	$C2$	0.92	Yes	39.7	0.80
OsH_2(bipyridine_I)	$C2$	0.88	Yes	43.5	0.73
OsH_2(bipyridine_Br)	$C2$	0.84	Yes	59.8	0.87
OsH_2(bipyridine_CH$_3$)	$C2$	0.83	Yes	61.8	0.90
OsH_2(bipyridine_CF$_3$)	$C2$	0.82	Yes	51.2	0.80
OsH_2(bipyridine_Cl)	$C2$	0.81	Yes	71.0	0.98
OsH_2(bipyridine_OH)	$C2$	0.72	Yes	80.9	1.26
OsH_2(bipyridine_F)	$C2$	0.63	No	82.1	1.32
OsH_2(bipyridine_CCH)	$C2$	0.65	Yes	94.0	1.33
OsH_2(bipyridine_H)	$P422$	0.52	No	88.5	1.33
OsH_2(bipyridine_CN)	$C2$	0.60	Yes	97.2	1.37

Table S4. Parameters of CMOFs materials being calculated: material type, ΔE, and the R-D coupling constant α in the valence band at the Γ point.

Material	Non-magnetic semiconductor	ΔE (meV)	α (eVÅ)
$RuCl_2$(bipyridine_I)	Yes	0.5	0.04
RuH_2(bipyridine_CN)	Yes	14.8	0.59

Table S5. Character table for the single and double group representatives of C_2 point group and the corresponding basis functions, given for the high symmetry k point Γ in C_2 Brillouin zone.

C_2	E	C_2	Linear functions rotations	Quadratic functions
A	1	1	z, R_z	x^2, y^2, z^2, xy

B	1	-1	x, y, R_x, R_y	yz, xz
C_2^D	E	$\bar{E}$	C_2	$\bar{E}C_2$
Γ_1	1	1	1	1
Γ_2	1	1	-1	-1
Γ_3	1	-1	i	-i
Γ_4	1	-1	-i	i

Table S6. Character table for the single and double group representatives of D_4 point group and the corresponding basis functions, given for the high symmetry k point Γ in $P422$ Brillouin zone.

D_4	E	$2C_4$	C_2	$2C'_2$	$2C''_2$	Linear functions rotations	Quadratic functions
A_1	1	1	1	1	1		x^2+y^2, z^2
A_2	1	1	1	-1	-1	z, R_z	z
B_1	1	-1	1	1	-1		x^2-y^2
B_2	1	-1	1	-1	1		xy
E	2	0	-2	0	0	$(x, y)\ (R_x, R_y)$	(xz, yz)
D_4^D	E	$\bar{E}$	$2C_4$	$2\bar{E}C_4$	$C_2, \bar{E}C_2$	$2C'_2, 2\bar{E}C'_2$	$2C''_2, 2\bar{E}C''_2$
Γ_1	1	1	1	1	1	1	1
Γ_2	1	1	1	1	1	-1	-1
Γ_3	1	1	-1	-1	1	1	-1
Γ_4	1	1	-1	-1	1	-1	1
Γ_5	2	2	0	0	-2	0	0
Γ_6	2	-2	$\sqrt{2}$	$-\sqrt{2}$	0	0	0
Γ_7	2	-2	$-\sqrt{2}$	$\sqrt{2}$	0	0	0

Table S7. The proportion of heavy elements in the valence band.

Material	Os	I
OsI_2(bipyridine_I)	0.43	0.16
$OsBr_2$(bipyridine_I)	0.50	0.003
$OsCl_2$(bipyridine_I)	0.54	0.002
OsF_2(bipyridine_I)	0.55	0.004
$Os(CN)_2$(bipyridine_I)	0.58	0.002
OsH_2(bipyridine_I)	0.65	0.003

Table S8. Effects of strong field ligands on R-D spin splitting. Here $E_g^{PBE+SOC}$ is the band gap, ΔE is the R-D energy of spin splitting, and α is the R-D coupling constant.

Material	$E_g^{PBE+SOC}$ (eV)	ΔE (meV)	α (eVÅ)
$Os(NCS)_2$(bipyridine_I)	1.56	8.9	0.11
$Os(NO_2)_2$(bipyridine_I)	1.69	13.0	0.28
$Os(PH_3)_2$(bipyridine_I)	Metal	-	-
$Os(CN)_2$(bipyridine_I)	1.30	34.9	0.48
$Os(CO)_2$(bipyridine_I)	Metal	-	-

The spectrochemical sequence for these strong field ligands is $NCS^- < NO_2^- < PH_3 < CN^- < CO$. The

calculation results show that the energy of spin splitting increases as the ligand field strength increases (see Table S8). Unfortunately, when the ligands are neutral molecules (PH_3 and CO), the system is metallic and does not meet our conditions.

References

1. Dresselhaus M S, Dresselhaus G, Jorio A. Group theory: application to the physics of condensed matter[M]. Springer Science & Business Media, **2007**.

2. C. J. Bradley and A. P. Cracknell, The Mathematical Theory of Symmetry in Solids Representation theory for point groups and space group, CLARENDON PRESS OXFORD 1972, P441-442

3. J. Richard, J. Joseph, C. Wang, A. Ciesielski, J. Weiss, P. Samori, V. Mamane, J. A. Wytko, *J. Org. Chem.*, 2021, **86**, 3356–3366.

4. G. R. Xu, Z. H. An, K. Xu, Q. Liu, R. Das, H. L. Zhao, Coord. *Chem. Rev.*, 2021, **427**, 213554.

5. T. Kambe, R. Sakamoto, K. Hoshiko, K. Takada, M. Miyachi, J. H. Ryu, S. Sasaki, J. Kim, K. Nakazato, M. Takata, H. Nishihara, *J. Am. Chem. Soc.*, 2013, **135**, 2462–2465.

6. T. Rodenas, I. Luz, G. Prieto, B. Seoane, H. Miro, A. Corma, F. Kapteijn, F. X. Llabrés i Xamena, J. Gascon, *Nat. Mater.*, 2015, **14**, 48–55.

7. S. C. Junggeburth, L. Diehl, S. Werner, V. Duppel, W. Sigle, B. V. Lotsch, *J. Am. Chem. Soc.*, 2013, **135**, 6157–6164.

8. Y. Sakata, S. Furukawa, M. Kondo, K. Hirai, N. Horike, Y. Takashima, H. Uehara, N. Louvain, M. Meilikhov, T. Tsuruoka, S. Isoda, W. Kosaka, O. Sakata, S. Kitagawa, *Science*, 2013, **339**, 193–196.

9. S. Zhao, Y. Wang, J. Dong, C. T. He, H. Yin, P. An, K. Zhao, X. Zhang, C. Gao, L. Zhang, J. Lv, J. Wang, J. Zhang, A. M. Khattak, N. A. Khan, Z. Wei, J. Zhang, S. Liu, H. Zhao, Z. Tang, *Nat. Energy*, 2016, **1**, 16184.

10. X. F Wang, L. Andrews, *J. Phys. Chem. A*, 2009, **113**, 551–563.

11. J. Multia, D. E. Kravchenko, V. Rubio-Giménez, A. Philip, R. Ameloot, M. Karppinen, *ACS Appl. Nano Mater.*, 2023, **6**, 827–831.

12. S. M. George, B. Yoon, A. A. Dameron, *Acc. Chem. Res.*, 2009, **42**, 498–508.

13. E. Ahvenniemi, M. Karppinen, *Chem. Commun.*, 2016, **52**, 1139–1142.

14. L. D. Salmi, M. J. Heikkilä, E. Puukilainen, T. Sajavaara, D. Grosso, M. Ritala, *Micropor. Mesopor. Mater.*, 2013, **182**, 147–154.

15. L. D. Salmi, M. J. Heikkilä, M. Vehkamäki, E. Puukilainen, M. Ritala, T. Sajavaara, *J. Vac. Sci. Technol.*, 2015, **33**, 01A121.